ACS APPLIED MATERIALS & INTERFACES

Research Article

www.acsami.org

Unidirectional Freezing of Ceramic Suspensions: In Situ X-ray Investigation of the Effects of Additives

Benjamin Delattre,*[,†,§] Hao Bai,[†] Robert O. Ritchie,[†,‡] Joël De Coninck,[§] and Antoni P. Tomsia[†]

[†]Materials Sciences Division Lawrence Berkeley National Laboratory, Berkeley, California 94720, United States

[‡]Department of Materials Science & Engineering University of California, Berkeley, California 94720, United States

[§]Laboratoire de Physique des Surfaces et Interfaces, Université de Mons, Mons 7000, Belgium

Supporting Information

ABSTRACT: Using in situ X-ray radiography, we investigated unidirectional freezing of titanium dioxide suspensions. We showed how processing additives, which are generally used for ice-templating, strongly modified freezing dynamics during the solidification process. We observed and identified different freezing regimes by varying the amount of dispersant, binder, or poly(ethylene glycol) (PEG). We demonstrated that because each regime corresponds to a given final structure understanding the particle motion and redistribution at the ice-front level was essential. We also examined the transition from a random particles-entrapment regime to a well-defined lamellar regime and proposed and discussed two mechanisms by which additives might affect the solidification process.

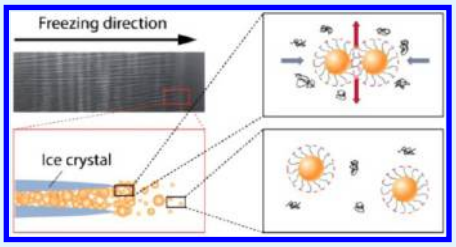

KEYWORDS: *freeze-casting, ice-templating, ice lens, unidirectional freezing, ice growth, freezing dynamics*

1. INTRODUCTION

Freeze-casting, also known as ice-templating, is a shaping technique able to create highly complex porous structures with morphologies that differ depending on the solvent used. The process consists of casting the slurry into a mold and freezing it unidirectionally through application of a thermal gradient. Under specific conditions during solidification, particles are expelled by the growth of an ice front and are entrapped between ice crystals. After removing ice by sublimation, a green body with a highly anisotropic structure is obtained and eventually consolidated by sintering. This environmentally friendly process has received a great deal of attention during the past decade.[1−6] Freeze-casting offers the advantage of being applicable to a wide range of solid materials such as ceramics, metals, or polymers. Potential applications include filters, catalyst supports, storage systems, solid-oxide fuel cells, electrodes, infiltrated ceramic−metal composites, or bone-graft substitutes. The process and its underlying mechanisms have been the subject of several recent comprehensive reviews.[3−6]

One of the most informative ways to examine the morphology of such freeze-cast structures, or scaffolds, is to use X-ray techniques. In recent years there has been significant progress in the fields of synchrotron X-ray radiography and tomography. This progress is linked with both advances in scientific computing that allow fast processing of complex algorithms to reconstruct objects in three dimensions and developments in CCD technology that enhance both resolution and time of acquisition. Deville et al. applied these techniques to investigate the solidification of alumina suspensions during the initial instant of freezing[7] followed subsequently by the so-called steady-state regime[8] and, finally, the instabilities at the solid−liquid interface.[9] More recently, the same group demonstrated the ability to use in situ 3D imaging to investigate the ice-crystal growth of colloidal silica suspensions.[10] The effect of supercooling and crystal growth during the initial freezing regime[11] was highlighted by Lasalle et al., who also described possible mechanisms to explain the redistribution of particles during the ice-templating process.[12]

During the last few years, the use of secondary additives to modify the crystallization behavior of the water has raised significant interest, as have the highly complex porous structures[13−15] that can be created with this approach. However, until recently, cooling rates and solid loading-content volume were the most common experimental parameters manipulated to control freezing dynamics in studies dealing with unidirectional freezing. It is now well-established that in the case of low-solid-content suspensions subjected to slow ice-front velocities (i.e., <1 μm/s) ice grows with a planar interface and rejects all foreign bodies into the remaining liquid phase.[16] This leads to a system where the two components, ice and particles, are completely separated at the completion of the freezing process. This technique is sometimes used for water purification[17] or for concentrating solutions in the food industry.[18] Final scaffolds that have a cellular or lamellar macromorphology with porosity oriented along the temperature gradient typically require faster cooling rates (1−25 °C/min) and higher solid contents (15−50% vol %), with those

Received: September 4, 2013
Accepted: December 17, 2013
Published: December 17, 2013

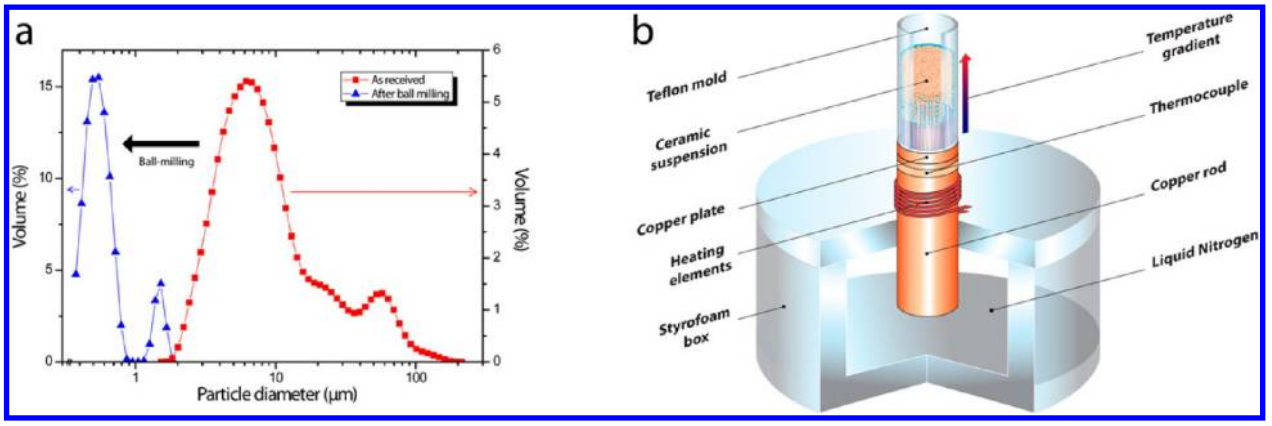

Figure 1. (a) Particle-size distribution of the TiO_2 powder, as received and after 20 h of ball-milling, is plotted as the particle volume distribution as a function of particle diameter. The D_{50} value, the value of the particle diameter at 50% in the cumulative distribution, decreases from 7.94 to 0.54 μm before and after ball-milling, respectively. (b) Schematic illustration of the homemade freezing stage. The ceramic suspension is cast into a Teflon mold, which is placed on a copper rod. Liquid nitrogen is contained in a Styrofoam box, and the cooling rate is remotely controlled by heating elements and a thermocouple linked to a power unit.

Table 1. Characteristics of the Suspensions under Study

dispersant concentration (wt %)	PEG concentration (wt %)	binder concentration (wt %)	slurry name
0.5	0	0	S1
		2	S2
	2	2	S3
1	0	0	S4
		2	S5
	2	2	S6
2	0	0	S7
		2	S8
	2	2	S9
0.5	0	0.1, 0.25, 0.5, 0.75, 1, 1.5, 3	S10–S16
0.5	0.1, 0.25, 0.5, 0.75, 1, 1.5, 3	0	S17–S23

ranges depending on the material. However, depending on the suspension characteristics, there is a critical value for solid content[19] or ice-front velocity above which particles will be entrapped randomly by the freezing front, resulting in loss of the lamellar structure.[16]

Processing additives such as dispersants and binders are commonly used to prepare suitable slurries. Dispersants are required to distribute ceramic particles homogeneously within the solvent and to ensure slurry stability over time, whereas binders are necessary to prevent the green body from collapsing before sintering. The aim of this work is to demonstrate that additives, even in small amounts, can strongly affect the freezing process. To study these effects on the dynamics of freezing, several TiO_2 suspensions were prepared with various amounts of binder, dispersant, and poly(ethylene glycol) (PEG). The role of PEG is to break the close alignment of the binder molecules and to deploy the coiled dispersant chains adsorbed at the surface of the particles. Synchrotron X-ray radiography experiments were used to follow particle motion in situ during solidification, at scales ranging from a few micrometers to several millimeters. Different freezing regimes were observed and identified. The transition from a random particle-entrapment regime to a well-defined lamellar regime was also investigated. In the following sections, we propose and discuss two mechanisms by which additives affect the solidification process.

2. RESULTS AND DISCUSSION

2.1. Slurry Preparation and Freezing. Titanium dioxide (TiO_2) powder was chosen because of the high level of contrast between the ice and the particle-rich phase. The total amount of TiO_2 powder in the slurry was arbitrarily set at 20 vol %. Slurries were ball-milled with zirconia balls for 20 h to deflocculate the powder and to allow adsorption of the dispersant onto the surface of the particles. Particle-size distributions were found to decrease significantly after ball-milling (Figure 1a), with the medium value D_{50} lowered from 7.94 to 0.54 μm. To illustrate separately the effect of each additive, nine slurries, designated S1–S9, were created with different amounts of dispersant, binder, and PEG (Table 1). Dispersant concentrations of 0.5 (S1–S3), 1 (S4–S6), and 2 wt % (S7–S9) were selected. These values are typical for systems having similar particle-size distributions, as reported in the literature.[20−24] In some slurries, a binder and/or PEG were added with a 2 wt % concentration. To illustrate more precisely the effects of the binder and PEG, 14 more slurries were created, designated S10–S23. Dispersant concentration was set at 0.5 wt %, whereas the concentrations of binder (S10–S16) and PEG (S16–S23) ranged from 0.1 to 3 wt %. An overview of all of the specific characteristics of each suspension is given in Table 1. Slurries were then degassed in a vacuum chamber before being transferred into a mold. Directional freezing was carried out with a homemade freezing stage (Figure 1b) using a cooling rate of 2.5 °C/min.

dx.doi.org/10.1021/am403793x | ACS Appl. Mater. Interfaces 2014, 6, 159−166

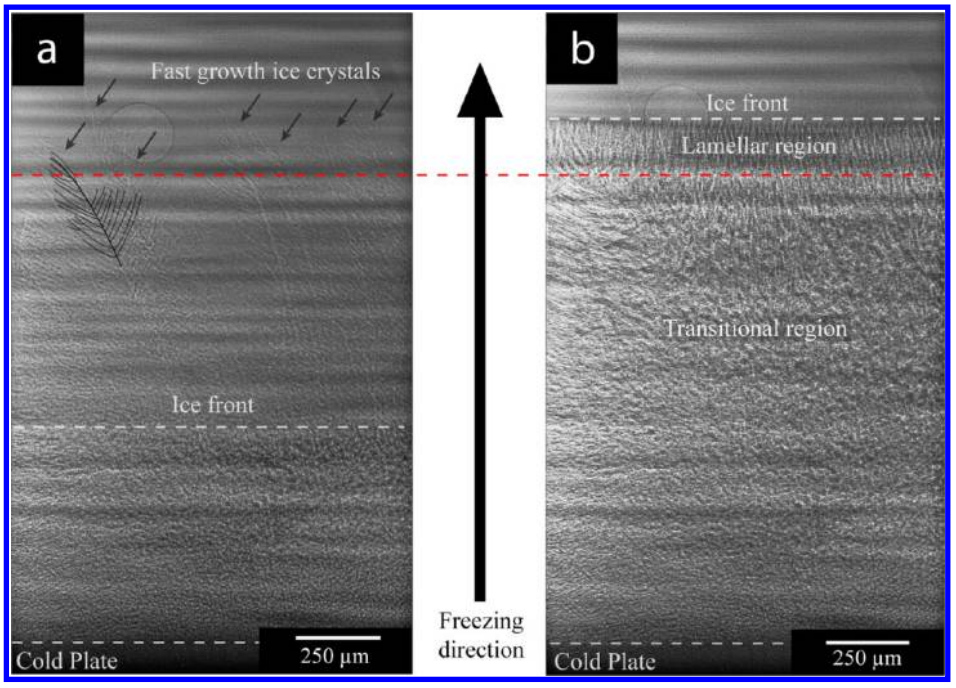

Figure 2. X-ray radiographs of a TiO_2 suspension (S3) during the start of the solidification process, taken at 0 and 3.2 s. (a) Three areas can be distinguished on this radiographic image. The dashed line at the top demarks the area where the first freezing regime of fast and highly dendritic ice crystals ended, the terminal points of which are identified by the small black arrows. The middle line indicates the position of the ice front during the second freezing regime. (b) Red dashed line at the top of the dendritic ice crystals region shows where a steady and lamellar regime begins. Despite careful precautions, the formation of small air bubbles was difficult to avoid, and such a bubble is seen in the upper left of both radiographs. However, this bubble did not seem to affect either the freezing regime or the shape and the speed of this interface.

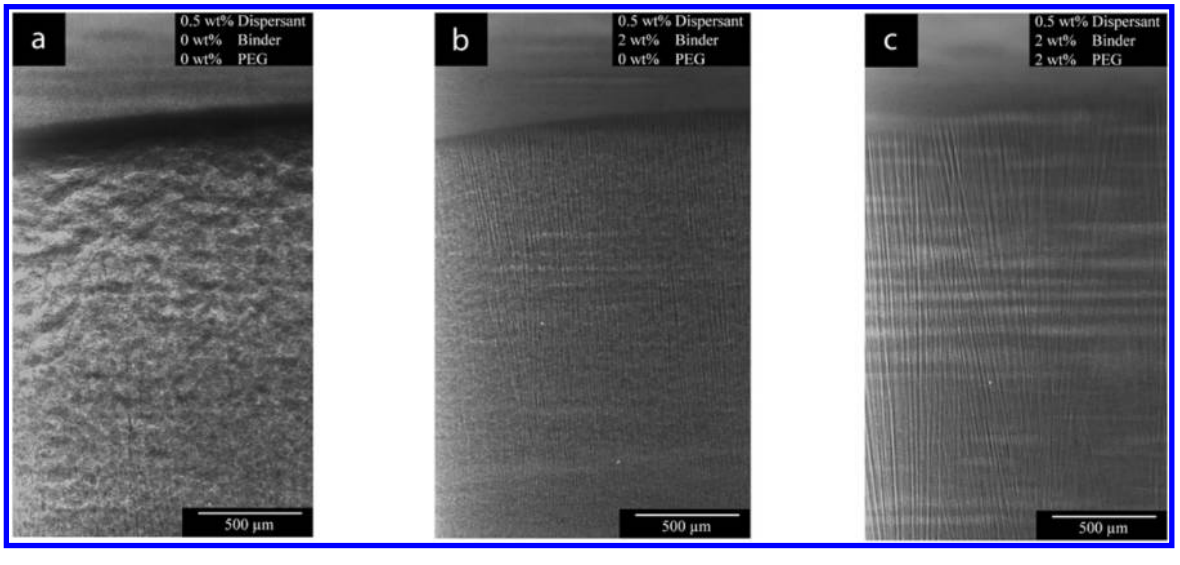

Figure 3. X-ray radiographs of different freezing regimes recorded during the steady-state solidification of TiO_2 suspensions. The pictures were taken 2 mm above the bottom of the mold. (a) For the S1 suspension with a concentration of 0.5 wt % of dispersant, a particle layer was observed that progressively thickened during the freezing process. This random-freezing regime led to a disordered final structure. (b) For the S2 suspension with 2 wt % additions of binder, only a small region of particle accumulation was present at the interface level, with the result that a coarse lamellar regime with partial dendritic components was obtained. (c) For the S3 suspension with 2 wt % additions of PEG, particles became well-redistributed immediately at the interface, and ice crystals adopted a needle-shaped structure ending with a sharp tip.

2.2. Initial Observations. *2.2.1. Typical Freezing Regimes Occurring during Freeze-Casting.* During unidirectional freezing of suspensions, three different freezing regimes are typically encountered.[7,8] The first regime, occurring at the start of the freezing process and resulting from the formation of a supercooled region,[11] consists of highly dendritic and extremely fast-growing ice crystals. This regime was successfully observed (Figure 2a) in each slurry listed in Table 1. However, because of the fast propagation of the ice crystals (>1 mm/s), our acquisition time was not fast enough to capture growth velocity.

Immediately following this fast regime, a second, slower regime occurred in the same zone. Here, ice-front progression was slow enough to be actively observed (Figure 2a). Finally, there evolved a third, steady-state, regime,[8] which extended

dx.doi.org/10.1021/am403793x | ACS Appl. Mater. Interfaces 2014, 6, 159−166

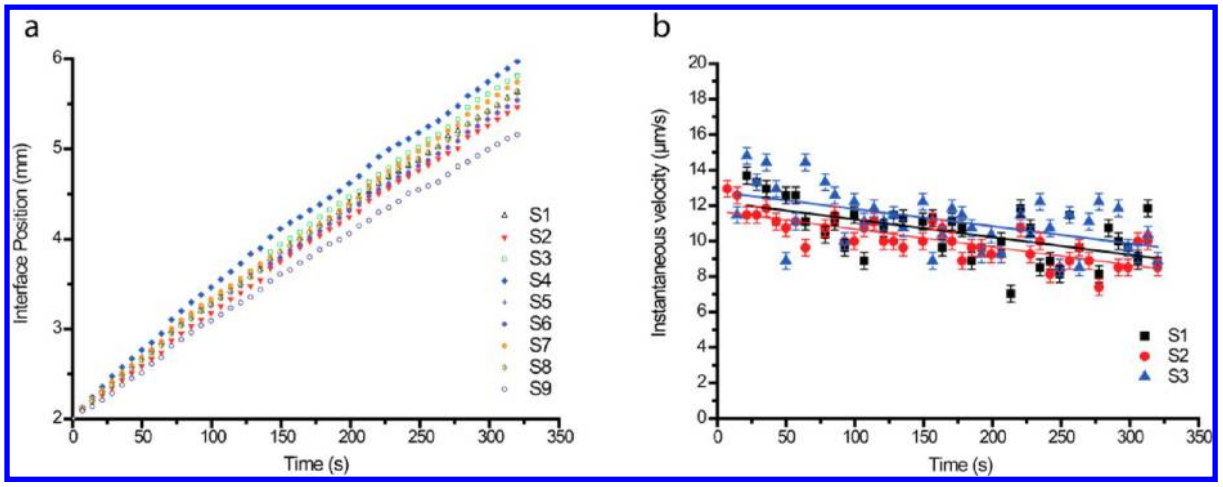

Figure 4. Freezing kinetics were investigated for slurries containing different amounts of additives; details of the slurries are listed in Table 1. (a) Ice-front positions as a function of time are plotted for slurries S1−S9. Each curve can be fitted with a second-degree polynomial regression. (b) Instantaneous interface velocity as a function of time for slurries S1−S3, which correspond to the three different freezing regimes, reported in Figure 3. Although large fluctuations of the instantaneous velocities can be observed for each of the three slurries, the average velocities, represented here by the dotted lines, do not differ by more than 2 μm/s during all of the steady-state freezing process. This implies that the changes in the freezing regimes are not related to the average velocity of the solid−liquid interface.

from the top of the fast-growing crystals to the top of the mold (Figure 2b). It is in this last regime that well-oriented and well-defined lamellar structures required for ice-templating applications are formed.

After sublimation, scaffolds usually exhibit two distinct regions. The first one, relatively dense and heterogeneous, corresponds to the transitional region,[11] whereas the second one corresponds to the lamellar region.

2.2.3. Effects of Additives on Freezing Kinetics. Initially, only slurries containing 0.5 wt % of dispersant (S1−S3) were investigated. For these three slurries, two distinctly different behaviors were observed. For the S1 slurry, which contained only dispersant, a fraction of the particles was rejected ahead of the ice front, creating a dense layer that became thicker as freezing progressed (250 μm at 4 mm from the bottom of the mold). The other fraction of the particles was periodically entrapped, leading to the formation of horizontal ice-banding patterns that are reminiscent of ice-lens patterns[25] (Figure 3a). Ice-lenses are usually observed in frozen soils and consist of ice crystals growing perpendicularly to the temperature gradient.[26,27] However, these patterns are generally encountered as a result of freezing at slower solidification velocities (i.e., <1 μm/s) than those measured here (i.e., >5 μm/s). This radiographic sequence is shown in Supporting Information Video S1.

When 2 wt % of binder was added (S2), a thinner particle layer was observed at the ice-front interface, as shown in Figure 3b and in the sequence of radiographs (Supporting Information Video S2). The thickness of this particle buildup was constant during the process and never exceeded 70 μm. As a result, the particles were well-redistributed in between ice-crystal tips. These initial experiments provided important insight into particle redistribution during the freeze-casting process. Additions of 2 wt % of binder agent induced a transition from a disoriented and random structure to a lamellar one. However, the ice crystals appeared to retain partially a dendritic shape. In a dendritic freezing regime, ice crystals develop branches that extend perpendicular to the primary direction of growth. The freezing regime shown on Figure 3b appears to present ice-crystal shapes similar to those obtained recently from fast X-ray tomography experiments.[10] In cases where two adjacent dendrites become connected, a disruption of a wall in the final structure may result.[12] This phenomenon is also likely to be responsible for the wide scatter in the compressive strength values of freeze-cast scaffolds previously reported in the literature. Finally, for the slurry containing 2 wt % of binder and 2 wt % of PEG (S3), ceramic particles were immediately and thoroughly redistributed at the interface, and no buildup of particles above the ice front was observed. Moreover, as shown in Figure 3c, the ice crystals adopted needle-shaped structures ending with sharp tips.

Among slurries S4−S9, further increases in the amount of the dispersant did not appear to affect the dynamics of freezing. Moreover, although horizontal instabilities are sometimes observed when using a specific particle size or interface velocity,[9] this phenomenon was not observed in any of our slurries.

The freezing kinetics were investigated by measuring ice-front positions as a function of time for slurries S1−S9. For each image in the sequence of radiographs, the position of the freezing front was measured manually using ImageJ software. Measurements were started at 2.5 ± 0.2 mm from the bottom of the mold, where the steady-state regime was already well-established. The results, plotted in Figure 4a, can be fitted with a second-degree polynomial regression. The instantaneous interface velocity was also plotted versus time (Figure 4b) for slurries S1−S3, corresponding to the three different freezing regimes reported previously. For each slurry, the graph revealed large fluctuations ranging from 7 to 15 μm/s. A slight decrease of the average velocities, represented here by the dotted lines, was also observed versus time. This can be explained through the imposed temperature conditions.[8] However, these average velocities followed the same trend and did not differ by more than 2 μm/s during the duration of the freezing process. These results showed clearly that, despite large differences in particle motion and redistribution observed among slurries S1, S2, and S3 (Figure 3), the changes in freezing regimes were not related to the velocity of the solid−liquid interface.

2.3. Transition between Random and Lamellar Regimes. On the basis of these initial results, additional

dx.doi.org/10.1021/am403793x | ACS Appl. Mater. Interfaces 2014, 6, 159−166

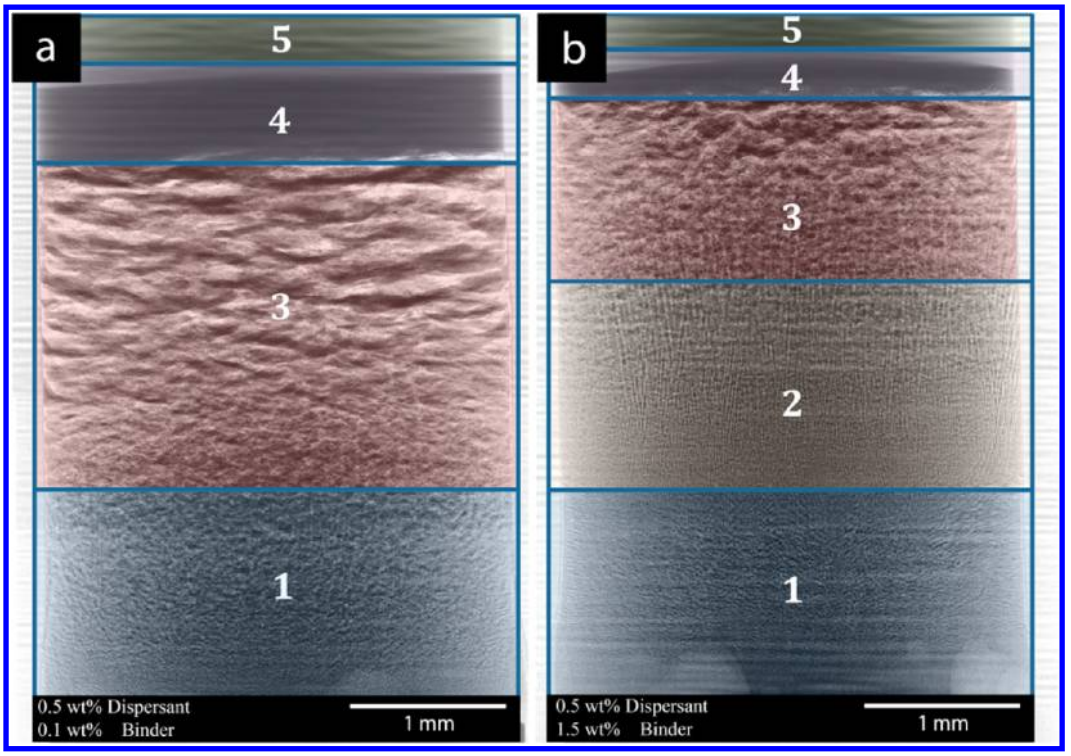

Figure 5. X-ray radiographic images of TiO_2 suspensions subjected to unidirectional freezing taken at equivalent times. (a) Freezing regime for a slurry (S10) containing 0.5 wt % of dispersant and 0.1 wt % of binder. In this regime, particles were entrapped or expelled randomly, with the result that a thick buildup of particles was formed ahead of the ice front. (b) Corresponding freezing regime for a slurry (S15) containing 0.5 wt % of dispersant and 1.5 wt % of binder. At this concentration, a lamellar freezing regime appeared immediately after the fast-growth regime. The length of this zone increased as the binder content was raised but was still followed by a random-freezing zone. These two pictures show that an increase in the amount of binder led to a deep modification in the morphology of the final frozen structure. The numbers refer to (1) the fast-freezing zone, (2) the lamellar regime zone, (3) the random-freezing zone, (4) the particle-buildup zone, and (5) the liquid phase. The freezing front is located at the interface between zones 3 and 4.

suspensions (S10–S23) were created with the objective of characterizing the transition between the random and the lamellar freezing regimes. Although the dispersant content was maintained at 0.5 wt %, both the binder and PEG concentrations were increased separately from 0.1 to 3 wt % (details are given in Table 1). In the case of the binder, a qualitative visualization of a radiographic sequence of images showed that an increase of concentration led to a regime transition. The radiographs shown in Figure 5a,b were taken at equivalent times. They revealed that when concentrations were lower than 0.5 wt %, a mushy freezing regime was observed: particles were entrapped or expelled randomly. Moreover, a thick buildup of particles formed ahead of the ice front, as shown in Figure 5a. At binder concentrations ranging between 0.5 and 1.5 wt %, a transition region could be detected when a lamellar zone was formed immediately after the fast-growth region (zone 2, Figure 5b). The differences in the freezing dynamics can be observed in the two radiographic image sequences provided as Supporting Information Videos S3 and S4.

The length of this zone increased in slurries with higher binder content, but it was still followed by a random-freezing zone. For each radiographic image in the sequence, the top and bottom positions of the particle buildup were measured using ImageJ software. It was shown that increasing the binder concentration from 0.1 to 1.5 wt % led to a two-fold reduction in the mean thickness of this particle-accumulation region (Figure 6). With binder concentrations at 2 wt % or higher, the random-freezing zone no longer forms so that beyond the fast-growth region only the lamellar region is evident along the sample length (Figure 3b). This transition is also observed in the case of PEG at a concentration of 0.5 wt %.

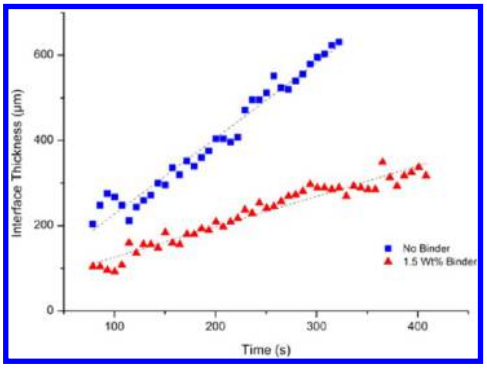

Figure 6. Evolution of the thickness of particle buildup at the interface. An increase in the binder concentration from 0 to 1.5 wt % led to a factor of 2 reduction in the mean thickness of the particles in the accumulation region.

2.4. Proposed Mechanisms. According to a proposed theoretical model,[3] a particle at the solid–liquid interface experiences both a repulsive force, $\overline{F}_R$, owing to the molecular van der Waals interactions of the freezing front, and an attractive force, $\overline{F}_\eta$, owing to the viscous drag (Figure 7). The repulsive force is a function of the particle radius and a balance between the different surface energies (particle–solid, particle–liquid, and solid–liquid). The attractive force is directly

dx.doi.org/10.1021/am403793x | ACS Appl. Mater. Interfaces 2014, 6, 159–166

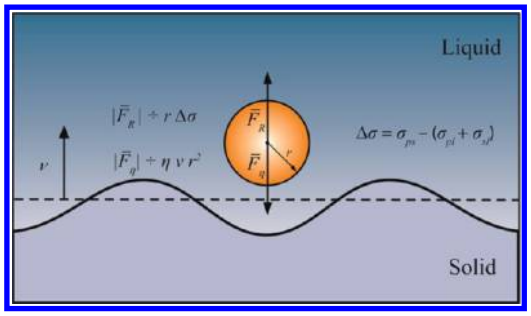

Figure 7. Adapted from Wegst et al.[3] According to a proposed theoretical model, a particle experiences at the solid–liquid interface both a repulsive force, $\overline{F}_R$, owing to the molecular van der Waals interactions of the freezing front, and an attractive force, $\overline{F}_\eta$, owing to viscous drag.

proportional to the viscosity of the slurry, the square of the particle radius, and to the ice-front velocity. The competition between these two forces will be determined by whether particles are rejected ahead the freezing front ($|\overline{F}_R| \gg |\overline{F}_\eta|$), are pushed in between the growing ice-crystals ($|\overline{F}_R| > |\overline{F}_\eta|$), or directly engulfed at the interface ($|\overline{F}_R| < |\overline{F}_\eta|$). However, this simple model was developed for a single particle. In fact, the balance between the two forces is a function of the solvent, which may or may not include additives, and also depends on the nature, amount, shape, state of dispersion, and particle-size distribution of the powder. It was recently reported[12] that increasing the dispersant content of alumina slurries (32 vol %) from 0.2 to 2 wt %, which results in a viscosity change from 10 to 90 mPa s, or increasing the cooling rate from 2 to 13 °C/min induced a transition from a random to a lamellar structure. We hypothesize that the viscosity and cooling-rate increases, both corresponding to an increase of the $|\overline{F}_\eta|$ value, might be responsible for the structural transition.

In our case, increasing the binder content from 0.1 to 3 wt % resulted in a linear increase of the slurries' viscosities from 8.8 to 25.3 ± 0.2 mPa s. Thus, the transition from a random to a lamellar freezing regime could be partially explained by using the viscosity argument. Indeed, for slurries containing less than 0.5 wt % of binder (S10–S12), $|\overline{F}_R| \gg |\overline{F}_\eta|$, the particle mobility was very high and, consequently, a buildup of particles was observed ahead the solid–liquid interface. Immediately after the fast-growth region, particles accumulated ahead the ice front until reaching the breakthrough concentration,[19] at which point they began to be engulfed. Between 0.5 and 1.5 wt % of binder (S12–S15), viscosities ranged between 11.6 and 13.7 ± 0.2 mPa s; the transition between the random regime and the lamellar regime was observed. At the beginning of the steady state, some particles were rejected ahead of the ice front, whereas others were trapped in between ice crystals. As a result, there remained a particle accumulation at the interface level. After some time, the breakthrough concentration was achieved, resulting in a disordered freezing regime. For slurries containing more than 2 wt % of binder, the viscosity was higher than 15.6 ± 0.2 mPa s, and particles directly accumulated in between the growing ice-crystals. As a result, a lamellar regime with no particle agglomeration ahead the freezing front was obtained.

However, the viscosity argument alone cannot explain the observed transition. Indeed, in the case of PEG, increasing its content from 0.1 to 3 wt % (S17–S23) induced a slight decrease in viscosities from 9.5 to 9.0 ± 0.2 mPa s. To explain the transition from a random to a lamellar freezing regime fully, we suggest that a mechanism known as depletion flocculation can account for the particle redistribution observed at the interface. In this study, the additives were added and stirred in the following order: dispersant, PEG, and, finally, the binder. Zeta potential measurements showed the dispersant adsorbed and negatively charged the particle surfaces. The resulting electrical double layer at the particle surface protected suspensions against flocculation. Both the binder, which is a nonionic polymer, as well as PEG remained dissolved in the water. Because they did not adsorb on the particle surface, there was around these particles a depletion layer where no polymer was present, as illustrated in Figure 8a.

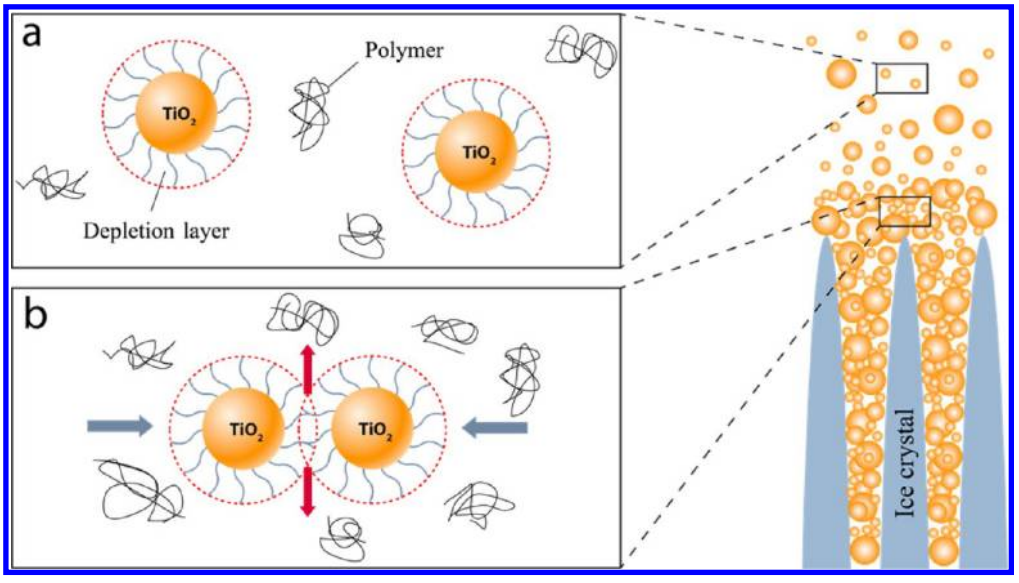

Figure 8. Schematic of the flocculation depletion mechanism. (a) Because the binder and lubricant do not adsorb on the particle surface, a depletion layer is formed around the particles. (b) Increasing additive concentration at the solid–liquid interface induces an overlap of the two depletion layers, excluding the polymer from the volume between particles. An osmotic pressure appears because of the polymer concentration gradient and acts as a driving force to move the particles until they aggregate. The resulting clusters can be finally trapped in between the ice crystals.

dx.doi.org/10.1021/am403793x | ACS Appl. Mater. Interfaces 2014, 6, 159–166

During the freezing process, pure ice crystals are growing into the liquid phase. This phenomenon has a tendency to drive water from the upper part of the ice front to the region where new ice crystals are forming. This causes an increase in the additives' concentration at the solid−liquid interface, which forces an increase in particle density. When the two depletion layers overlap, the polymer is excluded from the volume between the particles. The result is the formation of a polymer concentration gradient, which creates osmotic pressure, a driving force acting on opposite sides of the particles, pushing them closer and closer until they aggregate (Figure 8b). When the osmotic force is greater than the electrostatic force between the particles, flocculation occurs. The resulting particle clusters then can be entrapped between the growing ice crystals. We suggest that this process, known as depletion flocculation,[28] is the mechanism responsible for the transition from a random to a lamellar regime. Indeed, when concentrations were lower than 0.5 wt % of binder (S10−S12) or PEG (S17−S19), flocculation did not occur, and particles were rejected ahead the ice front, forming a thick interface (Figure 5a). This behavior led to the formation of a random structure. Concentrations of 0.5−1.5 wt % of binder (S12−S15) or PEG (S19−S22) were generally too low to allow all of the particles to flocculate, although some of them did, however, and were deposited between ice crystals, whereas others were expelled ahead of the ice front. Because of this partial rejection, the particle concentration at the interface was increased; on reaching the breakthrough concentration, a disordered structure eventually formed (Figure 5b). For binder or PEG concentrations of 2 wt % or greater, the flocculation-depletion mechanism was totally effective and only a buildup of small, consistently sized particles was observed at the interface as well as a lamellar regime (Figure 3b). Although the depletion-flocculation mechanism proposed here has several similarities to that described by Lasalle et al.,[12] major differences exist. For example, no depletion zone, either ahead of or behind the freezing front, was observed in any of the slurries investigated in this study.

An alternative mechanism that can increase the stabilization of the interface must also be considered. All of the compounds present here are soluble in water but have a very low solubility in ice. During the solidification process, additives are thus expelled from growing ice crystals and concentrate near the zone surrounding the ice-crystal tips. This increase in concentrations tends to lower the freezing temperature of the water and, consequently, stabilize the supercooled interface.

3. CONCLUSIONS

We have investigated in situ the role of additives in influencing the dynamics of the solid−liquid interface during the process of freeze-casting. By using a set amount of ceramic powder and a given cooling rate while changing the amount of processing additives, different freezing regimes were identified independently of the ice-front velocity. We report here how additives played a crucial role in the freezing dynamics and thus may affect the final integrity of the structure. On the basis of this study, the following conclusions can be made:

- Like in many ceramic shaping routes, a good and homogeneous dispersion of particles is required. However, minimal viscosity levels, usually related to the best states of dispersion, do not necessarily yield the freezing regime most suitable for ice-templating applications.
- Adding binder or PEG induces a transition from a disoriented and random structure to a lamellar structure of ceramic scaffolds.
- A depletion mechanism can account for the particle redistribution at the interface and is proposed as a possible mechanism.
- Although this work provides several insights about particle redistribution during ice-templating, more research is needed to explain and understand in detail all of the mechanisms involved. For instance, supercooling and supersaturation might also play key roles in the process.

4. EXPERIMENTAL SECTION

Slurry Preparation. Commercially available titanium dioxide TiO_2 (Sigma-Aldrich) was chosen as a powder. Aquazol polymer (ISP) with a molecular weight of 50 000 g/mol was used as a binder, poly(ethylene glycol) PEG 300 (Sigma-Aldrich), as a lubricant, Darvan C-N (R.T. Vanderbilt Co.), as a dispersant, and Milli-Q water, as a solvent.

Slurry Characterization. Particle-size distributions were measured using a laser diffraction particle-size analyzer (Beckman-Coulter LS 230). Suspension viscosities were measured at 1 ± 0.5 °C with a cone−plate viscometer (Brookfield LV-DV-II+ PRO with CPE-42 spindle) connected to a conventional cooling bath. Suspensions were transferred from the ball-milling container to the cup of the viscometer in less than 5 min. They were first presheared at 38.4 s^{-1} for 30 s and then left to rest for 30 s before the measurement was performed at the constant shear rate of 76.8 s^{-1}.

Freezing Stage. The freezing stage consisted of a cylindrical Teflon mold that was placed onto a copper cold finger; the temperature, and hence the cooling rate, was controlled using liquid nitrogen with a thermocouple linked to a power unit and ring heater. Suspensions were cast into the mold, taking care to avoid air-bubble entrapment; cooling rates were then set at 2.5 °C/min starting from ambient temperature.

X-ray Radiography. Synchrotron X-ray radiography experiments were carried out on beamline 8.3.2 at the Advanced Light Source (Berkeley, CA). Samples were scanned with a 24 keV monochromatic beam and imaged with a PCO-Edge CCD camera at 2560 × 2160 pixels resolution. A field of view of 3 mm was obtained using a 5× lens and a voxel size of 1.7 μm, with images captured with an acquisition rate ranging from 0.125 to 1 Hz depending on the objective of the experiment.

When the slurry is exposed to X-rays, it absorbs part of the beam energy, primarily from the presence of TiO_2 nanoparticles in the water; because this energy is converted into heat, it can potentially affect the solidification process. If the beam exposition is intermittent, then it can cause local and periodic modifications[10] in the temperature gradient that directly determines the speed of the ice front and can thus change the pore-size and wall-size distributions. During our experiments, however, molds containing slurries were exposed permanently to the beam to keep the temperature gradient constant; other suspensions were frozen without beam irradiation, and a single radiograph was taken at the end of the process. Qualitative comparison of the two sets of images confirmed that the X-ray exposures used did not affect the freezing kinetics.

■ ASSOCIATED CONTENT

Supporting Information

X-ray radiography videos of different freezing regimes recorded during the steady-state solidification of TiO_2 suspensions and SEM image of TiO_2 powder after 20 h of ball-milling. This material is available free of charge via the Internet at http://pubs.acs.org.

dx.doi.org/10.1021/am403793x | ACS Appl. Mater. Interfaces 2014, 6, 159−166

AUTHOR INFORMATION

Corresponding Author

*E-mail: bdelattre@lbl.gov.

Notes

The authors declare no competing financial interest.

ACKNOWLEDGMENTS

This work was supported by the Mechanical Behavior of Materials Program at Lawrence Berkeley National Laboratory and by the U.S. Department of Energy, Office of Basic Energy Sciences, Materials Sciences and Engineering Division, under contract no. DE-AC02-05CH11231. We acknowledge support of the X-ray tomography beamline 8.3.2 at the Advanced Light Source (ALS) at Lawrence Berkeley National Laboratory, which is also supported by the DOE's Office of Basic Energy Sciences under the same contract number.

REFERENCES

(1) Deville, S.; Saiz, E.; Nalla, R. K.; Tomsia, A. P. *Science* **2006**, *311*, 515−518.
(2) Fukasawa, T.; Deng, Z. Y.; Ando, M.; Ohji, T.; Goto, Y. *J. Mater. Sci.* **2001**, *36*, 2523−2527.
(3) Wegst, U. G.; Schecter, M.; Donius, A. E.; Hunger, P. M. *Philos. Trans. R. Soc., A* **2010**, *368*, 2099−2121.
(4) Deville, S. *Materials* **2010**, *3*, 1913−1927.
(5) Deville, S. *Adv. Eng. Mater.* **2008**, *10*, 155−169.
(6) Gutiérrez, M. C.; Ferrer, M. L.; del Monte, F. *Chem. Mater.* **2008**, *20*, 634−648.
(7) Deville, S.; Maire, E.; Lasalle, A.; Bogner, A.; Gauthier, C.; Leloup, J.; Guizard, C. *J. Am. Ceram. Soc.* **2009**, *92*, 2489−2496.
(8) Deville, S.; Maire, E.; Lasalle, A.; Bogner, A.; Gauthier, C.; Leloup, J.; Guizard, C. *J. Am. Ceram. Soc.* **2009**, *92*, 2497−2503.
(9) Deville, S.; Maire, E.; Bernard-Granger, G.; Lasalle, A.; Bogner, A.; Gauthier, C.; Leloup, J.; Guizard, C. *Nat. Mater.* **2009**, *8*, 966−972.
(10) Deville, S.; Adrien, J.; Maire, E.; Scheel, M.; Di Michiel, M. *Acta Mater.* **2013**, *61*, 2077−2086.
(11) Lasalle, A.; Guizard, C.; Leloup, J.; Deville, S.; Maire, E.; Bogner, A.; Gauthier, C.; Adrien, J.; Courtois, L. *J. Am. Ceram. Soc.* **2012**, *95*, 799−804.
(12) Lasalle, A.; Guizard, C.; Maire, E.; Adrien, J.; Deville, S. *Acta Mater.* **2012**, *60*, 4594−4603.
(13) Munch, E.; Saiz, E.; Tomsia, A. P.; Deville, S. *J. Am. Ceram. Soc.* **2009**, *92*, 1534−1539.
(14) Deville, S.; Viazzi, C.; Leloup, J.; Lasalle, A.; Guizard, C.; Maire, E.; Adrien, J.; Gremillard, L. *PloS One* **2011**, e26474-1−e26474-6.
(15) Deville, S.; Viazzi, C.; Guizard, C. *Langmuir* **2012**, *28*, 14892−14898.
(16) Waschkies, T.; Oberacker, R.; Hoffmann, M. J. *Acta Mater.* **2011**, *59*, 5135−5145.
(17) Lorain, O.; Thiebaud, P.; Badorc, E.; Aurelle, Y. *Water Res.* **2001**, *35*, 541−547.
(18) Shapiro, J. *Science* **1961**, *133*, 2063−2064.
(19) Shanti, N. O.; Araki, K.; Halloran, J. W. *J. Am. Ceram. Soc.* **2006**, *89*, 2444−2447.
(20) Fu, Q.; Rahaman, M. N.; Dogan, F.; Bal, B. S. *J. Biomed. Mater. Res., Part B* **2008**, *86*, 125−135.
(21) Sofie, S. W.; Dogan, F. *J. Am. Ceram. Soc.* **2001**, *84*, 1459−1464.
(22) Waschkies, T.; Oberacker, R.; Hoffmann, M. J. *J. Am. Ceram. Soc.* **2009**, *92*, S79−S84.
(23) Deville, S.; Saiz, E.; Tomsia, A. P. *Biomaterials* **2006**, *27*, 5480−5489.
(24) Deville, S.; Saiz, E.; Tomsia, A. P. *Acta Mater.* **2007**, *55*, 1965−1974.
(25) Anderson, A. M.; Worster, M. G. *Langmuir* **2012**, *28*, 16512−16523.
(26) Peppin, S. S. L.; Elliott, J. A. W.; Worster, M. G. *J. Fluid Mech.* **2006**, *554*, 147−166.
(27) Style, R. W.; Peppin, S. S.; Cocks, A. C.; Wettlaufer, J. S. *Phys. Rev. E: Stat., Nonlinear, Soft Matter Phys.* **2011**, *84*, 041402-1−041402-12.
(28) Jenkins, P.; Snowden, M. *Adv. Colloid Interface Sci.* **1996**, *68*, 57−96.